Biochemical Engineering Journal 178 (2022) 108297

Contents lists available at ScienceDirect

Biochemical Engineering Journal

journal homepage: www.elsevier.com/locate/bej

Flux balance analysis for overproduction of organic acids by *Synechocystis* sp. PCC 6803 under dark anoxic condition

Kshitija Japhalekar, Sumana Srinivasan, Ganesh Viswanathan *, K.V. Venkatesh *

Department of Chemical Engineering, Indian Institute of Technology Bombay, Powai, Mumbai 400076, India

ARTICLE INFO

Keywords:
Succinate
Dark anoxic
Flux balance analysis
Central carbon metabolism
Organic acids

ABSTRACT

Cyanobacteria have recently been considered as potential organisms for metabolic engineering with an objective to improve its ability to synthesize biofuel precursors and other value-added products. A modified version of the genome-scale metabolic model of *Synechocystis* sp. PCC 6803 model organism was used to theoretically demonstrate the flux distribution in the central carbon metabolism towards optimal accumulation of organic acids, namely succinate, acetate, lactate and malate. We further validate the model using experimental data reported by Hasunuma et al. *Met. Engg. Comm.*, 2016, **3**, 130–141 for organic acid synthesis under dark anoxic conditions from glycogen accumulated during photoautotrophic growth conditions by sequestering atmospheric CO_2. We show that key limiting factors are redox balance causing gluconeogenesis, availability of CO_2 and channeling of carbon flux to TCA cycle, in addition to the rate of breakdown of glycogen. Sodium bicarbonate supplementation enhances succinate production flux by eliminating the CO_2 limitations for the phosphoenolpyruvate (PEP) to oxaloacetate biochemical reaction catalyzed by PEP carboxylase. A combined strategy of supplementation with $NaHCO_3$ and increased temperature can only offer ~25% of the theoretical maximum succinate production. We suggest possible metabolic pathway interventional approaches to improve the succinate productivity.

1. Introduction

Natural production of various organic acids such as succinate, lactate, malate using cyanobacteria has gained importance in recent times [1–3]. Cyanobacteria has become a candidate organism since genetic and metabolic engineering approaches are feasible. This has led to use of cyanobacteria in synthesis of various biofuel precursors and industrially relevant products [4–9]. Model organisms such as *Escherichia coli* or *Saccharomyces cerevisiae*, give high yield of organic acids than cyanobacteria but require sugars or biomass feed-stocks as carbon sources for fermentation [10,11]. However the ability of cyanobacteria to metabolize atmospheric CO_2 for its growth and accumulation of metabolites is an added advantage from the perspective of green synthesis of organic acids [12]. Through its core metabolic pathways, it can route the carbon from either CO_2 or a suitable carbohydrate to these acids under dark conditions [13,14]. Being a photoautotrophic microorganism, cyanobacteria employs photosynthesis machinery to accumulate various macromolecules such as glycogen [15–19].

One of the promising strategies employed recently is to first grow cyanobacteria in light conditions and subsequently expose it to dark anoxic environment [20–23]. While cyanobacteria accumulate glycogen by efficient uptake of atmospheric CO_2 when grown in light, the carbon in the accumulated hydrocarbon is utilized to synthesize organic acids in dark anoxic environment [20,24]. Among the cyanobacteria, *Synechocystis* sp. PCC6803 (*SC* 6803) is an organism with rich genome scale data available and is a model for studying algal systems.

Metabolism in *SC* 6803 was first characterized by employing a metabolic model that accounted for the biochemical reactions in the central metabolic pathway [25,26]. Subsequently, several detailed genome-scale metabolic models (GSMMs) such as *iJN678* [27] were systematically reconstructed by considering the organism's growth under different conditions [27–32]. Saha et al. [33] improved these *SC* 6803 metabolic network reconstructions by integrating various observations such as presence of TCA bypass, fatty acid biosynthesis into the *iSyn731* comprehensive model. *iSyn731* model subject to biomass maximization yielded flux ranges consistent with the experimental measurements [33]. Building upon these reconstructions, particularly via enhancing *iSyn731* model [33] by gap-filling in pathways such as

* Corresponding authors.
E-mail addresses: ganeshav@iitb.ac.in (G. Viswanathan), venks@iitb.ac.in (K.V. Venkatesh).

https://doi.org/10.1016/j.bej.2021.108297
Received 17 June 2021; Received in revised form 24 November 2021; Accepted 1 December 2021
Available online 3 December 2021
1369-703X/

photorespiration, the updated GSMM *iSynCJ816* of *SC* 6803 predicted the experimental observations [34].

A recent study successfully demonstrated that by alternating light and dark conditions, atmospheric CO_2 sequestered by *SC* 6803 to accumulate glycogen during light condition can be subsequently metabolized to produce organic acids such as succinate under dark anoxic environment [21,22,35]. Such an approach yielded ~0.27 mmol of succinate per mmol of equivalent glucose from glycogen when *SC* 6803 was grown in NH_4Cl rich media. It should be noted that under dark anoxic conditions the organism accumulated other organic acids as well namely lactate, acetate and malate. This indicated that there is scope for improving utilization of carbon in glycogen towards synthesizing succinic acid. Overexpression of *ppc* gene that codes for phosphoenolpyruvate (PEP) carboxylase enzyme yielded ~0.32 mmol of succinate per equivalent glucose from glycogen, a 20% increase. This overexpression facilitated the channeling of carbon to oxaloacetate and thereby improving the succinate yield. Although a strategy for improving yield is demonstrated in the study, the underlying metabolic state is not known.

A question therefore arises whether the succinate yield can be improved further. Knowledge of the underlying metabolic state is necessary to address this question and can offer insights into the same. The objective of this study is to delineate strategies to enhance yield of organic acids such as succinate by *SC* 6803 exposed to dark anoxic conditions after grown in light. In order to achieve this objective, we consider performing flux balance analysis on a genome-scale metabolic model of *SC* 6803 [27] to predict the underlying state that may correspond to the experimental conditions described in Refs. [21,22]. Using the model [27] and by mimicking the dark anoxic experimental condition, we predict the conditions that may lead to higher yields of the organic acids.

2. Methods

2.1. Data extraction

Data for secreted and intracellular metabolite accumulation during dark anoxic fermentation of *SC* 6803 from Hasunuma et al. [21,22] were extracted. Note that the *SC 6803* was first grown under light conditions with atmospheric CO_2 as the sole carbon source in 5 mM NH_4Cl or 5 mM $NaNO_3$ rich media. The harvested cells were fermented under dark anoxic conditions to synthesize organic acids. In particular, using the biochemical reactions of the central carbon metabolic pathway in which the measured metabolites participate in (Table S1, Supplementary information), we extracted the time-varying accumulation levels of 5 secreted and 22 intracellular metabolites (Table S2, Supplementary information) from Hasunuma et al. [21,22]. Using WebPlotDigitizer [36], the concentration of various metabolites at different time points (0 h, 3 h, 6 h, 24 h, 48 h, 72 h and 96 h) was used to estimate the metabolite pool. Similar data for the case of mutant strain over-expressing *ppc* gene under three different temperatures were also used [22]. Note that this mutant strain over-producing Phosphoenolpyruvate (PEP) carboxylase was achieved by transforming *SC* 6803 with pSKtrc-slr0168/sII0920 plasmid causing amplification of *ppc* gene [21]. Succinate, acetate and lactate rates were calculated for the effect of sodium biocarbonate ($NaHCO_3$) supplementation in dark anoxic condition at 30 °C and 37 °C (Text S1, Supplementary information). These rates were also calculated for different concentrations (50, 100, 200 and 300 mM) $NaHCO_3$ supplementation, and were incorporated in the model as constraints.

2.2. Flux estimation for metabolic reactions

Average accumulation rates of both intracellular and extracellular metabolites were estimated between 6 h and 96 h using the corresponding experimentally measured dynamic levels. These rates were further scaled with the mean dry cell weight under dark conditions to estimate the specific accumulation rates in *mmol/gDW/hr*. Reaction fluxes were calculated for glycolysis, TCA cycle, Calvin cycle and pentose phosphate (PP) pathway including 31 intracellular metabolites participating in 33 reactions (Tables S1 and S2, Supplementary information). Note that, for every metabolite, a balance between its production and consumption via different biochemical reactions was used for this purpose. Details of these calculations are in Text S1, Supplementary information.

2.3. Genome-scale metabolic model

The genome-scale metabolic model (GSMM) of *SC* 6803 namely *iJN678* [27] was used for flux balance analysis. The model comprises of 864 biochemical reactions, 795 metabolites and 678 genes with gene-protein-reaction (GPR) associations for each reaction. These reactions are divided along 54 subsystems in 4 different cellular compartments like extracellular, cytoplasm, periplasm and thylakoid. Note that *iJN678* included biochemical reactions corresponding to ionic, NADH and NADPH balances, and ATP production and consumption. The GSMM was modified by introducing biochemical reactions corresponding to transport reaction for lactate and to exchange reactions for lactate and glycogen. The reactions are

$$LACtex : D-lactate[e] \rightleftharpoons D-lactate[p] \quad (1)$$

$$LACtpp : H[p] + D-lactate[p] \rightleftharpoons H[c] + D-lactate[c] \quad (2)$$

$$EX\_glycogen : bglycogen[c] \rightleftharpoons \quad (3)$$

$$EX\_lactate : D-lactate[e] \rightleftharpoons \quad (4)$$

where [c], [p] and [e] denotes metabolites present in cytoplasm, periplasm and extracellular respectively. Metabolites involved in the above reactions but not present in the *iJN678* were included in the modified genome-scale metabolic model (mGSMM). Note that no other biochemical reactions in *iJN678* were modified or deleted.

2.4. Flux balance analysis

An objective function was set to maximize glycogen uptake for FBA simulation (COBRApy 0.13.4 [37] in Python 3.6.6) estimated by linear programming [38]. To mimic the experimental dark anoxic conditions, the model was constrained by setting glucose, sodium bicarbonate, photon, and oxygen uptake rates to zero. Further, as these conditions do not favor growth, all biomass accumulation reactions were constrained to zero. mGSMM along with these constraints were employed in the flux balance analysis to simulate the model-based flux distribution under various conditions. A comparison of the fluxes predicted by mGSMM and *iSynCJ816* [34] is presented in Text S3, Supplementary information for a sample case. Experimental fluxes (estimated using the method specified above) were compared with the model predicted maximum and minimum fluxes simulated using flux variability analysis (FVA) [39,40]. mGSMM model was also used for FBA simulations for analyzing flux distribution due to variation in temperature. mGSMM being a genome-scale metabolic model, the topology of the underlying metabolic network itself does not change due to variation in temperature. For the case of the FBA simulations to study the effect of $NaHCO_3$ supplementation, in addition to the constraints specified above, the sodium bicarbonate uptake rate was constrained with that estimated from experimental data. (Details pertaining to the availability of SBML version of the mGSMM and the COBRApy script are Text S4, Supplementary information.).

2.5. Calculation of kinetic parameters

Relationship between the accumulation rates of various organic acids and the $NaHCO_3$ concentration was deduced by using, as a model, Haldane [41] or Hill equation, respectively given by

Table 1
Glycogen uptake rate and yield of organic acids production under different experimental conditions. The mutant strains were grown in NH_4Cl rich media.

Experimental conditions	Glycogen uptake rate (mmol/gDW/h)	Yield (mmol/mmol glucose utilized by glycogen)			
		Succinate	Acetate	Malate	Lactate
$NaNO_3$	0.0067	0.2327	2.2937	0.0165	0.1073
NH_4Cl	0.0079	0.2671	2.1621	0.0150	0.1056
ppc overexpression at 30 °C	0.0141	0.3190	2.3012	Nd	0.0291
ppc overexpression at 35 °C	0.0341	0.1700	2.5514	Nd	0.0702
ppc overexpression at 37 °C	0.0451	0.1294	2.4886	Nd	0.1674

$$\nu = \frac{V_{max} S}{K_S + S + (S^2/K_I)} \tag{5}$$

or

$$\nu = \frac{V_{max} S^n}{K_{0.5}^n + S^n} \tag{6}$$

where ν is the accumulation rate of the organic acid at a certain $NaHCO_3$ (substrate) concentration S, V_{max} is the maximum rate (mmol/gDW/h), K_S is the substrate saturation constant (mM), K_I is the substrate inhibition constant (mM), $K_{0.5}$ is the substrate concentration (mM) at half-maximal rate and n is the Hill coefficient. Values for these parameters and root mean square error (R^2) were estimated using the function 'Solver', Microsoft Excel 2013.

3. Results

3.1. Flux balance analysis of SC 6803 under dark anoxic fermentation

The rates of glycogen uptake and accumulated organic acids for wild-type cells grown in NH_4Cl and $NaNO_3$ [21,22] are listed in Table 1 (Section 2). In both cases, while most of the carbon from glycogen is utilized for producing acetate, the remaining were distributed among succinate, lactate and malate. Succinate production is twice as that of lactate, which in turn is ten times that of malate.

We employed flux balance analysis (FBA) on the modified genome-scale metabolic model (mGSMM) to estimate the range of feasible fluxes for the intracellular metabolic pathways including breakdown of glycogen (GLCP2) that match the constraints set (Section 2). These fluxes are contrasted with those estimated from the experimental data (Section 2) for the case of wild-type cells grown in NH_4Cl (Fig. 1) and $NaNO_3$ (Fig. S2, Supplementary information). Fluxes estimated from the

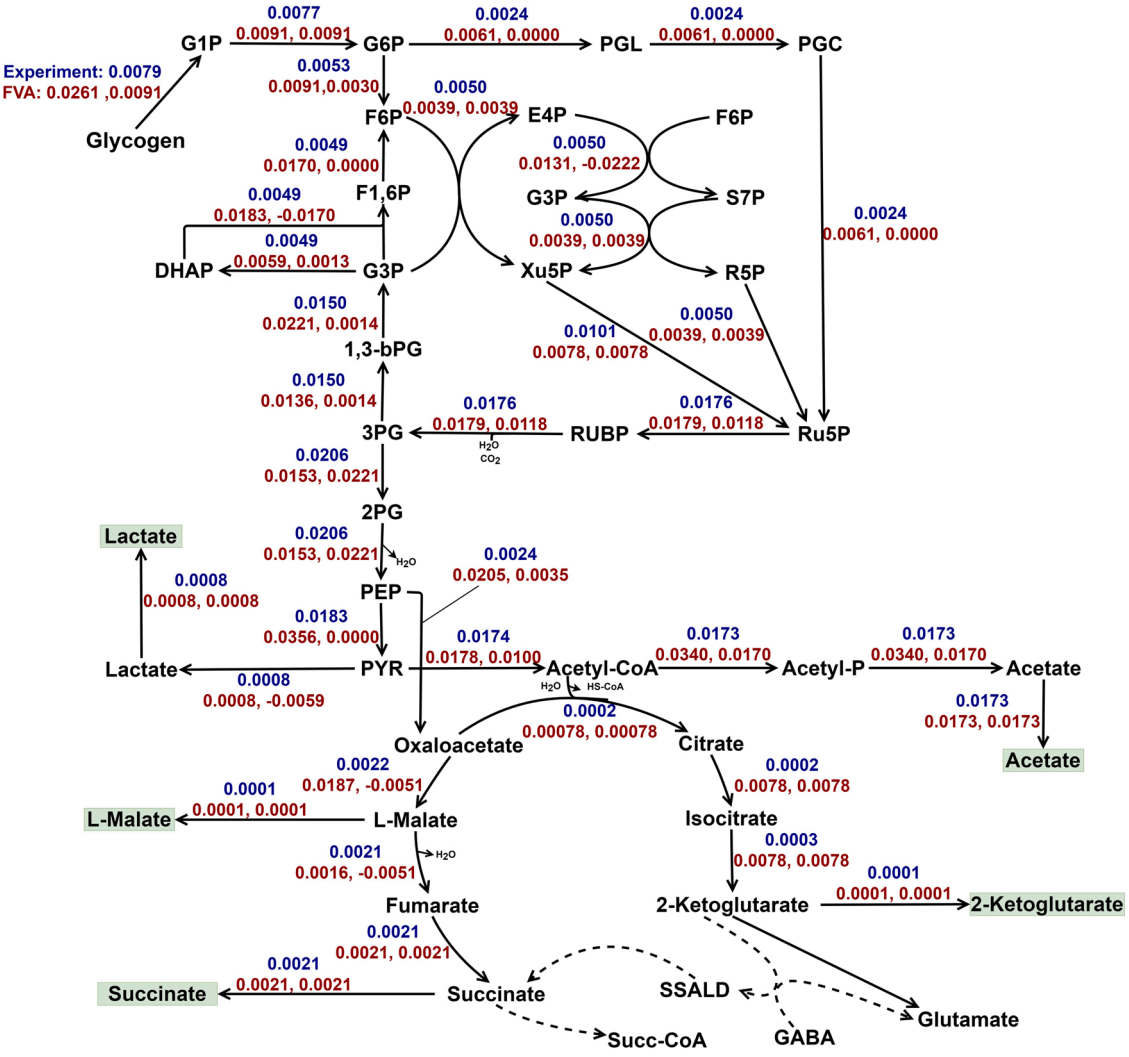

Fig. 1. Flux distribution map of the central carbon metabolic pathway comparing the experimental fluxes (blue) and those model predicted maximum and minimum (red) given by flux variability analysis under dark anoxic conditions for *SC* 6803 grown in NH_4Cl rich media. Fluxes are in mmo/gDW/h.

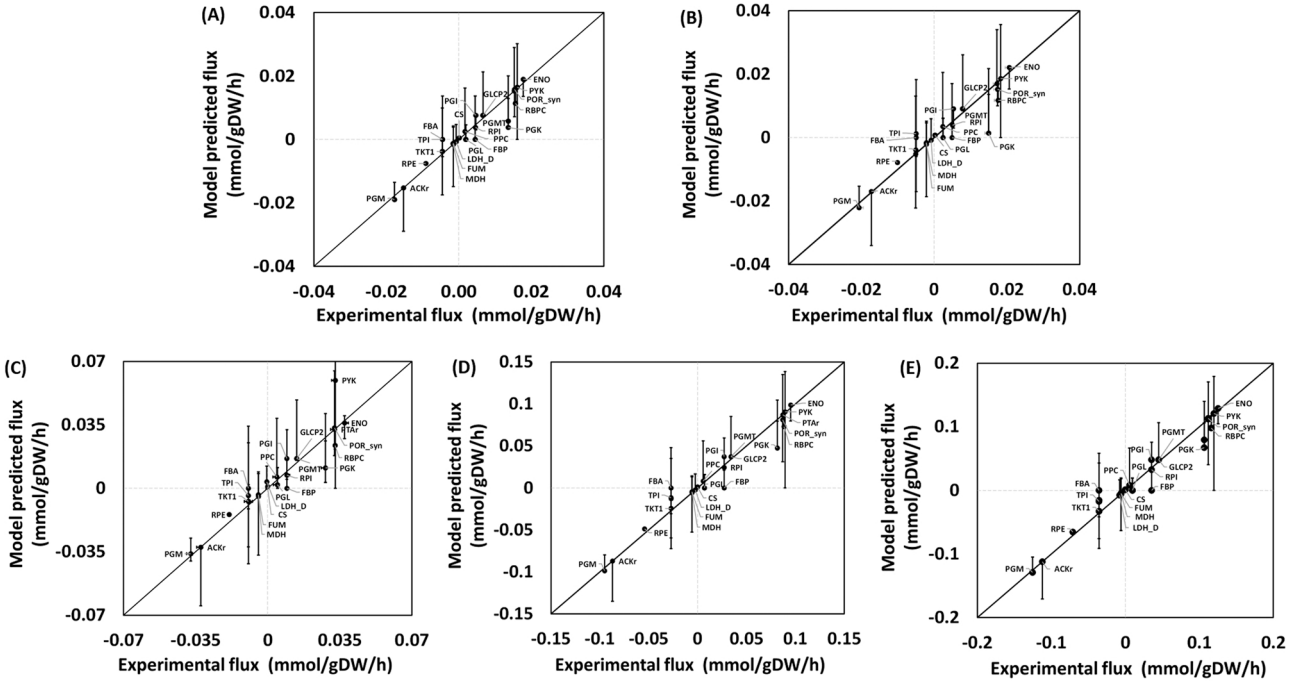

Fig. 2. Comparison of the model predicted flux and those estimated from experimental data for intracellular reactions under dark anoxic conditions for wild-type *SC* 6803 grown in (A) $NaNO_3$ and (B) NH_4Cl rich media. A similar comparison for the *ppc* gene overexpressing mutant strains under dark anoxic conditions at temperature C) 30 °C, D) 35 °C, E) 37 °C. Error bars represents maximum and minimum fluxes estimated using FVA. Certain reactions labeled are as specified in Table S1.

metabolite accumulation data were in the FVA range predicted by the FBA of the mGSMM. In particular, 30% of the carbon from glycogen is channeled via the Pentose Phosphate (PP) pathway. A fraction of this carbon is recycled back to make the EMP pathway operational suggesting partial gluconeogenesis may be occurring in the cells. Note that the NADPH and NADH redox balance, which are included in the mGSMM, necessitates gluconeogenesis. CO_2 generated during the formation of acetyl CoA from pyruvate (reaction POR_syn) is utilised for converting PEP to oxaloacetate (OAA) using PEP carboxylase and for D-ribulose 1,5-bisphosphate (RUBP) to 3PG using ribulose biphosphate carboxylase (RBPC) in Calvin cycle. The model was able to capture the experimentally reported observation that conversion from 2-ketoglutarate to succinate in the TCA cycle is non-functional. This suggests that TCA cycle may be truncated with the reductive pathway being operational for producing succinate from OAA. Fluxes estimated using FBA for these two conditions are contrasted with the corresponding experimentally determined quantities in Fig. 2 (a and b). The mGSMM predicted fluxes matched well with those from experimental accumulation data. The succinate production is through the reductive pathway for which conversion of PEP to OAA catalyzed by the PEP carboxylase, coded by *ppc* gene, is the key step.

We next considered the effect of the accumulation rates due to the overexpression of *ppc* gene in *SC* 6803 grown in NH_4Cl and subsequently subject to dark anoxic fermentation. In the case of *ppc* gene mutant strain, the glycogen uptake rate (Section 2) increased by ~ 1.75 fold at 30 °C and significantly upon increase in temperature to 35 °C (by ~ 4.25 fold) and 37 °C (by ~ 5.6 fold) (see Table 1). Overexpression of *ppc* gene led to 20% and 10% increase in yield of succinate and acetate, respectively. On the other hand, the yield of lactate was only 30% of that achieved in the case of wild-type and malate was undetected. Further, increase in temperature for the mutant strain decreased succinate yield with a concomitant increase in lactate yield. The FBA analysis showed an enhanced reductive pathway caused by *ppc* gene overexpression and thereby leading to an increased succinate yield. The model predicted fluxes at three different temperatures (Suppl. Figs. S3–S5) matched with the corresponding ones estimated using experimental data (Fig. 2c–e).

3.2. Nodal analysis for flux distribution

In the central carbon pathway, the key five nodes that control channeling of carbon are glucose-6-phosphate (Glu6-p), 3-phosphoglycerate (3PG), PEP, pyruvate (PYR), and OAA (Fig. 3). The glucose from glycogen breakdown is used in the form of glucose-1-phosphate to form Glu6-p which in turn is converted to gluconolactone-6-phosphate (6PGL) via PP pathway and fructose-6-phosphate (Fru-6-P) via glycolysis. In the wild-type cases, the flux split ratio between these two reactions is 0.3 and 0.7, respectively. On the other hand, for the case of mutant at 30°C, the split ratio marginally changes to 0.34 and 0.66. However, upon increasing temperature, the split ratio changes significantly to 0.2 and 0.8. This suggests that, for the case of mutant, temperature significantly affects the channeling of carbon through the glycolysis and PP pathways.

The next key nodal metabolite is 3PG which is synthesized from RUBP through the Calvin cycle and further is converted to 1,3-bisphosphoglycerate (1,3-bPG) via gluconeogenesis and to 2-phosphoglycerate (2PG) via glycolysis. For all the conditions, ~ 43% of carbon is recycled back through gluconeogenesis and remaining further downstream. This 43% recycle is for redox balance, as noted in the previous section. Next important node is PEP. While 10% carbon in PEP, synthesized from 2PG, is channeled to OAA in the case of wild-type, the overexpression of *ppc* gene in cells grown at 30 °C led to a marginal increase to 12%. However, further increase in temperature resulted in reduction of carbon channeled to OAA with a concomitant decrease in the succinate yield (Table 1).

At the PYR node, marginal channeling of carbon occurs towards producing lactate. The decrease in flux to PYR caused by *ppc* overexpression in cells grown at 30 °C results in reduction of lactate production. Upon increasing temperature, the lactate production levels is similar to that in wild-type. This implies that the increase in flux to OAA due to *ppc* overexpression is compensated by the decrease in lactate

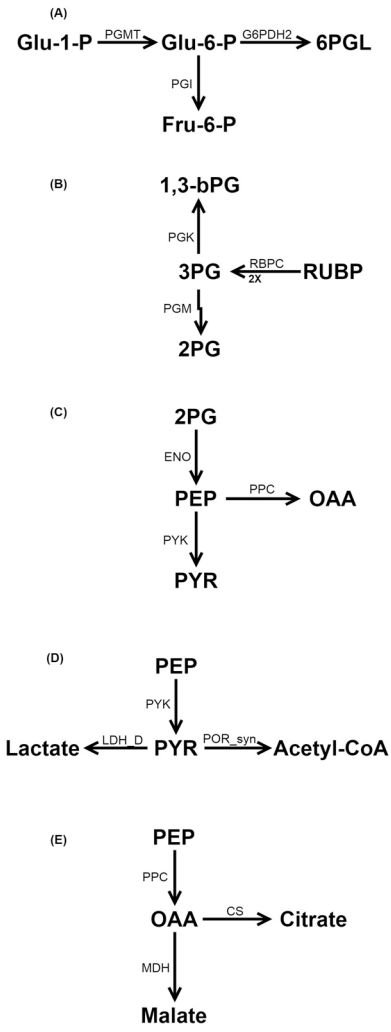

Reaction	$NaNO_3$	NH_4Cl	30°C PPCox	35°C PPCox	37°C PPCox
PGMT	0.98 (100)	0.99 (100)	1.00 (100)	1.00 (100)	1.00 (100)
G6PDH2	0.28 (29)	0.31 (31)	0.34 (34)	0.21 (21)	0.21 (21)
PGI	0.70 (71)	0.68 (68)	0.66 (66)	0.79 (79)	0.79 (79)

Reaction	$NaNO_3$	NH_4Cl	30°C PPCox	35°C PPCox	37°C PPCox
PGK	2.04 (43)	1.90 (42)	1.99 (43)	2.39 (46)	2.36 (46)
RBPC	4.70 (100)	4.50 (100)	4.64 (100)	5.18 (100)	5.14 (100)
PGM	2.66 (57)	2.62 (58)	2.65 (57)	2.79 (54)	2.78 (54)

Reaction	$NaNO_3$	NH_4Cl	30°C PPCox	35°C PPCox	37°C PPCox
ENO	2.66 (100)	2.62 (100)	2.65 (100)	2.79 (100)	2.78 (100)
PYK	2.41 (90)	2.32 (89)	2.33 (88)	2.62 (94)	2.65 (96)
PPC	0.25 (9)	0.30 (11)	0.32 (12)	0.17 (6)	0.13 (4)

Reaction	$NaNO_3$	NH_4Cl	30°C PPCox	35°C PPCox	37°C PPCox
PYK	2.41 (100)	2.32 (100)	2.33 (100)	2.62 (100)	2.66 (100)
POR_syn	2.30 (95)	2.21 (96)	2.30 (99)	2.55 (97)	2.49 (94)
LDH_D	0.11 (5)	0.11 (4)	0.03 (1)	0.07 (3)	0.17 (6)

Reaction	$NaNO_3$	NH_4Cl	30°C PPCox	35°C PPCox	37°C PPCox
PPC	0.25 (100)	0.30(100)	0.32 (100)	0.17 (100)	0.13 (100)
CS	0.01 (4)	0.02 (7)	0.00	0.00	0.00
MDH	0.24 (96)	0.28 (93)	0.32 (100)	0.17 (100)	0.13 (100)

Fig. 3. Important nodes in central metabolic pathway controlling carbon channeling and the fluxes (normalized by glycogen uptake rate) corresponding to the reactions in which they are involved. Numbers in the brackets capture the percentage of flux channeled from the node via different reactions.

synthesis. Further downstream, at the OAA node, reductive pathway converting OAA to malate dominates (99%) over the oxidative pathway of the TCA cycle. As it has been indicated previously, this is the primary mechanism that governs the accumulation of succinate from glycogen under dark anoxic conditions.

3.3. Improving yields of organic acids

Experimentally validated mGSMM, as demonstrated in the previous section, was next used to identify strategies for further improvement of the synthesis of the organic acids. In order to achieve this, we constrained the glycogen uptake rate to that estimated from experimental data and set the objective function of the FBA to maximize organic acid under dark anoxic, no growth conditions. Further, both oxidative and reductive branches of TCA cycle were kept functional.

The normalized flux distribution of the biochemical reactions corresponding maximization of succinate is shown in Fig. 4. The maximum theoretical yield for succinate is 0.47, which was ~ 1.5 times larger than the yield obtained for the case of *ppc* overexpression at 30 °C from experiments. The flux distribution indicated that maximum succinate theoretical yield will demand no lactate and malate synthesis, and a reduced acetate accumulation (~ 60% decrease as compared to experimental observations for the case of *ppc* overexpression at 30 °C). Further, the extent of gluconeogenesis decreases significantly indicating lower redox demand. Interestingly, the mGSMM revealed that maximum theoretical yield is dominated by the oxidative pathway unlike the reductive pathway being dominant in the case of *ppc* overexpression at 30 °C. Note that the carbon is channeled through the γ-aminobutyric acid (GABA) shunt and *not* through the regular TCA cycle. This could be due to a reduced redox demand necessary for maximization of the succinate.

The maximization of succinate requires that glucose from the breakdown of glycogen is entirely channeling into the glycolytic pathway (Fig. 5A). Further, the recycle of flux at 3PG reduces by 75% as compared to the *ppc* overexpression at 30 °C. These ensure that the redox demand for the PP pathway and the extent of gluconeogenesis is proportionately reduced. At the next important node PEP, the flux split up ratio for PPC reaction is 30% as compared to 10% for the case of *ppc* overexpression at 30 °C. This suggests that more overexpression of *ppc* gene is essential to further improve the yield of succinate. At PYR, flux to LDH_D reaction is negligible indicating no production of lactate, which is desirable as separation post synthesis can be avoided. At OAA, the carbon is primarily channeled through the oxidative pathway (~ 77% to CS reaction) and the rest results in synthesis of aspartate. Note that this was not observed in the experiments as the reductive pathway is dominant in the TCA cycle.

We next considered maximization of acetate, lactate and malate. The experiments suggest a maximum yield of 2.55 (Table 1) achieved for the case of *ppc* overexpression at 35 °C. The maximum theoretical yield achieved by setting maximization of acetate as the objective function for

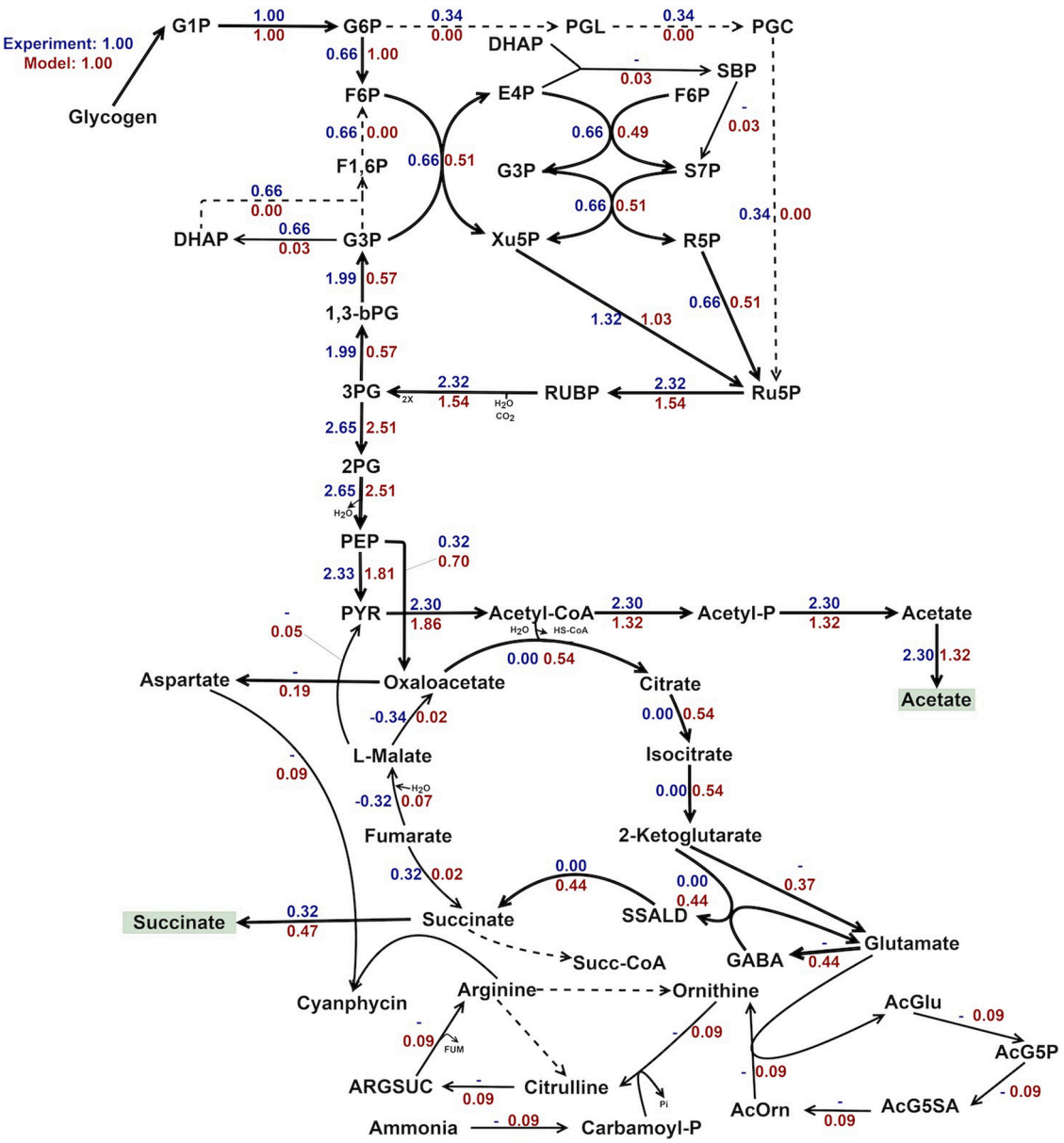

Fig. 4. Normalized flux distribution map corresponding to theoretical maximum succinate contrasted with that estimated from experimental data for *ppc* gene overexpressing mutant *SC* 6803 at 30 °C under dark anoxic conditions. Fluxes were normalized with the corresponding absolute glycogen breakdown flux of 0.0141 mmol/gDW/h.

the FBA of the mGSMM is 3 (Fig. S6, Supplementary information). This can also be observed in the nodal analysis (Fig. 5). On the other hand, maximization of lactate leads to a flux distribution that would make the cells homo-lactate, wherein all carbon from glycogen is channeled to lactate via glycolysis, which is also clearly captured in the nodal analysis (Figs. 5 and S7, Supplementary information). The maximization of malate offers a flux distribution that could lead to a significant increase in its synthesis (Fig. S8, Supplementary information). This increase is due to carbon channeled through PP pathway, although reduced by half as that for the case of *ppc* overexpression at 30 °C. The nodal analysis shows that primary channel for carbon from Glu-6-P is the glycolysis pathway and only 17% of the flux going through the PP pathway (Fig. 5A). Further, a unique feature is that 18% of the input flux towards PYR is through lactate via dihydroxyacetone phosphate (DHAP). The nodal analysis around OAA shows that the flux is primarily through PPC reaction, suggesting that *ppc* overexpression facilitates malate synthesis (Fig. 5E). Further downstream, the reductive pathway of the TCA cycle is found to be operational. Under these conditions, the accumulation of acetate is reduced. Note that while PEP to OAA biochemical reaction is catalyzed by PEP carboxylase, CO_2 is also a substrate for this reaction. Thus, even if *ppc* gene can be overexpressed, the flux through this reaction could be limited by the availability of CO_2.

3.4. Sodium bicarbonate supplementation enhances organic acid production

Sodium bicarbonate supplementation is one possible strategy to increase the CO_2 pool in *SC* 6803 [22]. Based on the estimate of the rate of organic acids from experimental data [22] at 30 °C and 37 °C when *SC* 6803 was supplemented with different concentrations of $NaHCO_3$ under dark anoxic conditions, the fluxes for succinate, acetate and lactate were deciphered (Section 2). The dependence of these fluxes on $NaHCO_3$ concentration at the two temperatures considered is shown in Fig. 6. For the case of succinate, a peak was observed at 200 and 100 mM $NaHCO_3$ supplement at 30 °C and 37 °C, respectively. We hypothesize that the decrease in the flux at higher $NaHCO_3$ concentrations could be due to

(A)

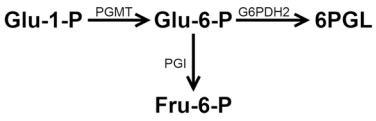

Reaction	Max. Succinate	Max. Malate	Max. Lactate	Max. acetate
PGMT	1.00 (100)	1.00 (100)	1.00 (100)	1.00 (100)
G6PDH2	0.00	0.17 (17)	0.00	0.00
PGI	1.00 (100)	0.83 (83)	1.00 (100)	1.00 (100)

(B)

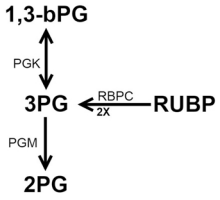

Reaction	Max. Succinate	Max. Malate	Max. Lactate	Max. acetate
PGK	0.57 (19)	0.03 (2)	2.00 (100)	3.00 (50)
RBPC	3.08 (100)	1.94 (98)	0.00	6.00 (100)
PGM	2.51 (81)	1.97 (100)	2.00 (100)	3.00 (50)

(C)

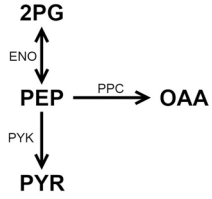

Reaction	Max. Succinate	Max. Malate	Max. Lactate	Max. acetate
ENO	2.51 (100)	1.97 (100)	2.00 (100)	3.00 (100)
PYK	1.81 (72)	1.38 (70)	2.00 (100)	3.00 (100)
PPC	0.70 (28)	0.59 (30)	0.00	0.00

(D)

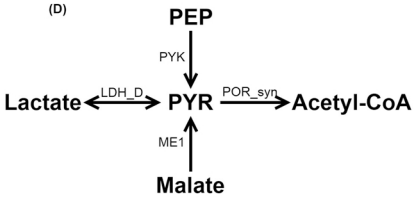

Reaction	Max. Succinate	Max. Malate	Max. Lactate	Max. acetate
PYK	1.81 (97)	1.38 (82)	2.00 (100)	3.00 (100)
POR_syn	1.86 (100)	1.68 (100)	0.00	3.00 (100)
LDH_D	0.00	0.30 (18)	2.00 (100)	0.00
ME1	0.05 (3)	0.00	0.00	0.00

(E)

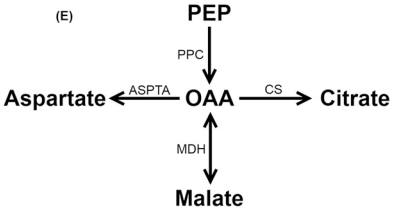

Reaction	Max. Succinate	Max. Malate	Max. Lactate	Max. acetate
PPC	0.70 (100)	0.59 (100)	0.00	0.00
CS	0.54 (77)	0.08 (14)	0.00	0.00
MDH	0.02 (3)	0.34 (58)	0.00	0.00
ASPTA	0.18 (26)	0.17 (29)	0.00	0.00

Fig. 5. Important nodes in central metabolic pathway controlling the carbon channeling and the fluxes (normalized by glycogen uptake rate) corresponding to the reactions in which they are involved for the cases of theoretical maximum succinate, malate, lactate and acetate production. Numbers in the brackets capture the percentage of flux channeled from the node via different reactions.

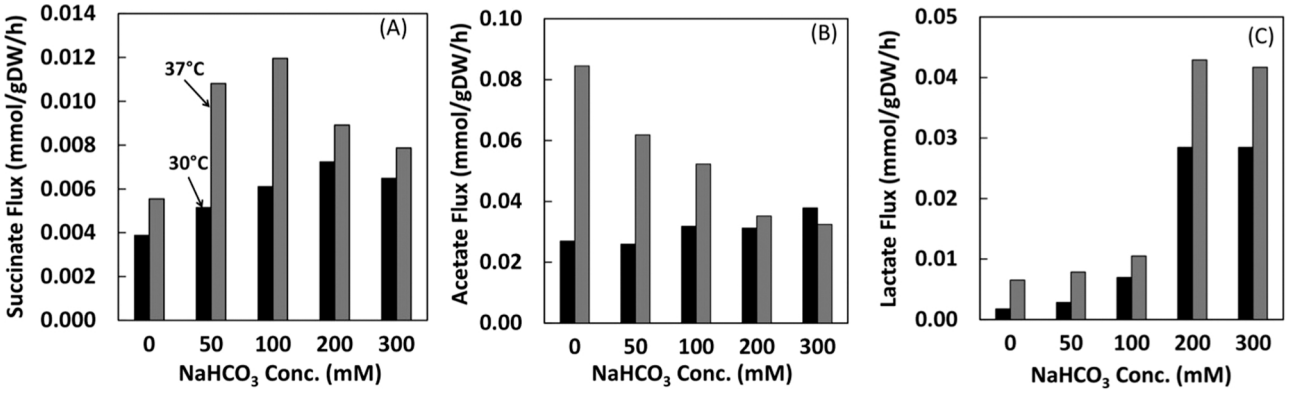

Fig. 6. Flux estimated for extracellular (A) succinate, (B) acetate and (C) lactate secreted by *SC* 6803 under dark anoxic conditions at 30 °C and 37 °C when supplemented with different concentrations of sodium bicarbonate. Note that for the sake of consistency, the data corresponding to zero concentration $NaHCO_3$ is based on those reported by Hasunuma et al. [22] for studying the effects of sodium bicarbonate supplementation.

Table 2
Kinetic parameters quantifying the organic acid production under dark anoxic condition with sodium bicarbonate supplementation. Haldane and Hill models are in Eqs. (5) and (6), respectively (Section 2).

Temperature (°C)	V_{max} (mmol/gDW/h)	K_S (mM $NaHCO_3$)	K_I (mM $NaHCO_3$)	R^2
Succinate: Haldane Model				
30	0.007	13.35	1.42×10^8	0.966
37	0.013	0.003	527.15	0.743
Acetate: Haldane Model				
30	0.042	30.62	1.90×10^{10}	1
37	0.076	0	225.06	1
Temperature (°C)	V_{max} (mmol/gDW/h)	$K_{0.5}$ (mM $NaHCO_3$)	n	R^2
Lactate: Hill Model				
30	0.43	2.21×10^3	1.33	1
37	3.08	1.42×10^4	1.11	0.989

the presence of an overall inhibition. On the other hand, for the case of acetate, with increasing $NaHCO_3$ concentration, while the flux increased marginally at 30 °C, interestingly a decreasing trend was observed at 37 °C which could perhaps be due to an inhibitory action. Flux increased with $NaHCO_3$ concentration for the case of lactate at both temperatures.

In order to quantify the effect of $NaHCO_3$ concentration on the fluxes of the organic acids, kinetic analysis was performed. Note that this kinetic analysis captures the overall $NaHCO_3$ dose response. Haldane model (Eq. (5)) was used, which includes inhibition terms, for quantifying succinate and acetate flux dependence on $NaHCO_3$ concentration. On the other hand, we employed Hill model (Eq. (6)) to capture the effect of $NaHCO_3$ on lactate flux. The parameters estimated are in Table 2 (Section 2). We note that, as expected, the V_{max} capturing the maximum rate increased with increasing temperature for all three acids. For the case of succinate and acetate, significant decrease in K_I with increasing temperature indicates the presence of strong inhibition at 37 °C. On the other hand, for the case of lactate, the values of the exponent, n, suggest that the sensitivity to $NaHCO_3$ concentration has decreased marginally with increasing temperature.

3.4.1. Flux balance analysis for sodium bicarbonate supplementation under dark anoxic condition

Rates calculated for extracellular acetate, lactate and $NaHCO_3$ along with measured glycogen uptake (Section 2) were constrained by maximizing extracellular succinate as the objective function in mGSMM. Note that flux towards biomass accumulation was kept open in mGSMM. However, no flux towards biomass was observed indicating the absence of growth in spite of the presence of $NaHCO_3$ as a carbon source under the dark anoxic conditions.

We first consider the case of secretion of organic acids by *SC* 6803 under dark anoxic conditions supplemented with different concentrations of $NaHCO_3$ at 30 °C. Normalized flux distributions on the central metabolic pathway for these concentrations are shown in Fig. 7. Interestingly, at all concentrations considered, while PP pathway largely remained unused, the flux to OAA is primarily recycled via L-malate to PYR resulting in the formation of significant quantities of acetate via acetyl-CoA. Rest of the flux in the reductive pathway of the TCA cycle results in secretion of succinate. Absence of flux from acetyl-CoA to citrate indicates that the oxidative pathway of the TCA cycle is inactive. Further, flux towards lactate is primarily through the alternative pathway via DHAP and not via the classical route involving pyruvate. Carbon channeling pattern through the central metabolic pathway at 37 °C (Fig. S9, Supplementary information) is similar to that observed for 30 °C.

Since sodium bicarbonate supplementation enhances secreted organic acids, we next investigate the extent of carbon sourced from $NaHCO_3$. Note that while $NaHCO_3$, which is completely utilized, adds to overall CO_2 pool. The carbon from it could either be distributed among various metabolites or be secreted. Depending upon the sodium bicarbonate supplementation concentration and the temperature, about 10–25% flux worth of carbon from $NaHCO_3$ is distributed to different metabolites in the pathway at 30 °C and 37 °C (Fig. 8). This indicates that carbon from $NaHCO_3$ contributed to the increased organic acids secretion when *SC* 6803 was supplemented with $NaHCO_3$ (Fig. 6). Other than a slight increase for 100 mM at 37 °C, increase in supplemented $NaHCO_3$ reduces the fraction of the carbon distributed into the metabolic pathway.

In order to distill out the effect of temperature and $NaHCO_3$ supplementation on the channeling of carbon through the central metabolic pathway, we next perform a nodal analysis using the estimated accumulation rates. Based on the flux distribution, key nodes channeling carbon flow towards production of organic acids are PEP, PYR, OAA, L-malate. The normalized fluxes channeled at these nodes as a function of temperature and $NaHCO_3$ concentrations are in Fig. 9. For both temperatures considered, while the flux distributed from PEP to PYR and OAA remained nearly poised up to 100 mM, at higher concentrations the carbon channeled to PYR nearly doubled indicating that the OAA route is less preferred (Fig 9A). In the presence of $NaHCO_3$, carbon reaching OAA junction is completely channelized into the reductive pathway (Fig. 9B) indicating that the oxidative pathway of the TCA cycle remains non-operational. Further, flux reaching L-malate is recycled to PYR and the remaining carbon ends up in Succinate via Fumarate. This recycled carbon accounts for about half of that reaching PYR at certain $NaHCO_3$ concentrations (Fig. 9C). Most of the carbon flux reaching PYR is utilized for producing acetate via acetyl-CoA (Fig. 9C). Nature of dependence of the extent of carbon recycle via L-Malate on the $NaHCO_3$ concentration could be dictating the peak observed in the succinate secretion. Further significant reduction in the recycle via L-malate at high concentrations and simultaneous doubling of flux from PEP to PYR could lead to enhanced acetate secretion at 200 mM and 300 mM (Fig. 6).

3.4.2. Improved sodium bicarbonate assisted organic acid secretion

We next asked a question if the secretion of organic acids can be further improved when $NaHCO_3$ supplement is provided. In order to answer this, in the mGSMM, we constrained the glycogen uptake rate to that estimated from experimental data and also the $NaHCO_3$ supplement to that used in experiments. We then set the objective function of the FBA to maximize organic acid under dark anoxic conditions with biomass accumulation kept open. Further, both oxidative and reductive branches of TCA cycle were kept functional. For the case of 100 mM $NaHCO_3$ supplementation, a comparison of the distribution of flux when organic acids were constrained to experimentally observed rates and with those when succinate was maximized showed that 4.25 fold improvement in the secreted succinic acid could be achieved (Fig. 10). The flux distribution further suggests that the extra carbon is sourced from $NaHCO_3$ by (a) reducing the CO_2 secretion from 72% to 50%, and (b) arresting the carbon recycle to PYR via L-malate and channeling carbon from DHAP to lactate via PYR to oxidative pathway of the TCA cycle. While the former aids in increasing the carbon availability, the latter ensures that carbon which would otherwise lead to formation of acetate and lactate are diverted to forming succinate.

4. Discussion

Cyanobacteria *Synechocystis* sp. PCC 6803 (*SC* 6803) has the ability to sequester atmospheric CO_2 and utilize the carbon for its growth. Our modified genome-scale metabolic model (mGSMM) revealed that the redox balance plays a crucial role in the experimentally observed flux distribution in the central carbon metabolic pathway. This drives partial gluconeogenesis upto ~ 43% in order to balance the NADH and NADPH, and thereby keeping the Calvin cycle operational. Further, mGSMM also predicted the experimentally observed feature that TCA cycle is truncated post 2-ketoglutarate and with the functioning of the reductive pathway being dominant. In order to enhance the flux through the reductive pathway, a common strategy is to overexpress *ppc* gene which

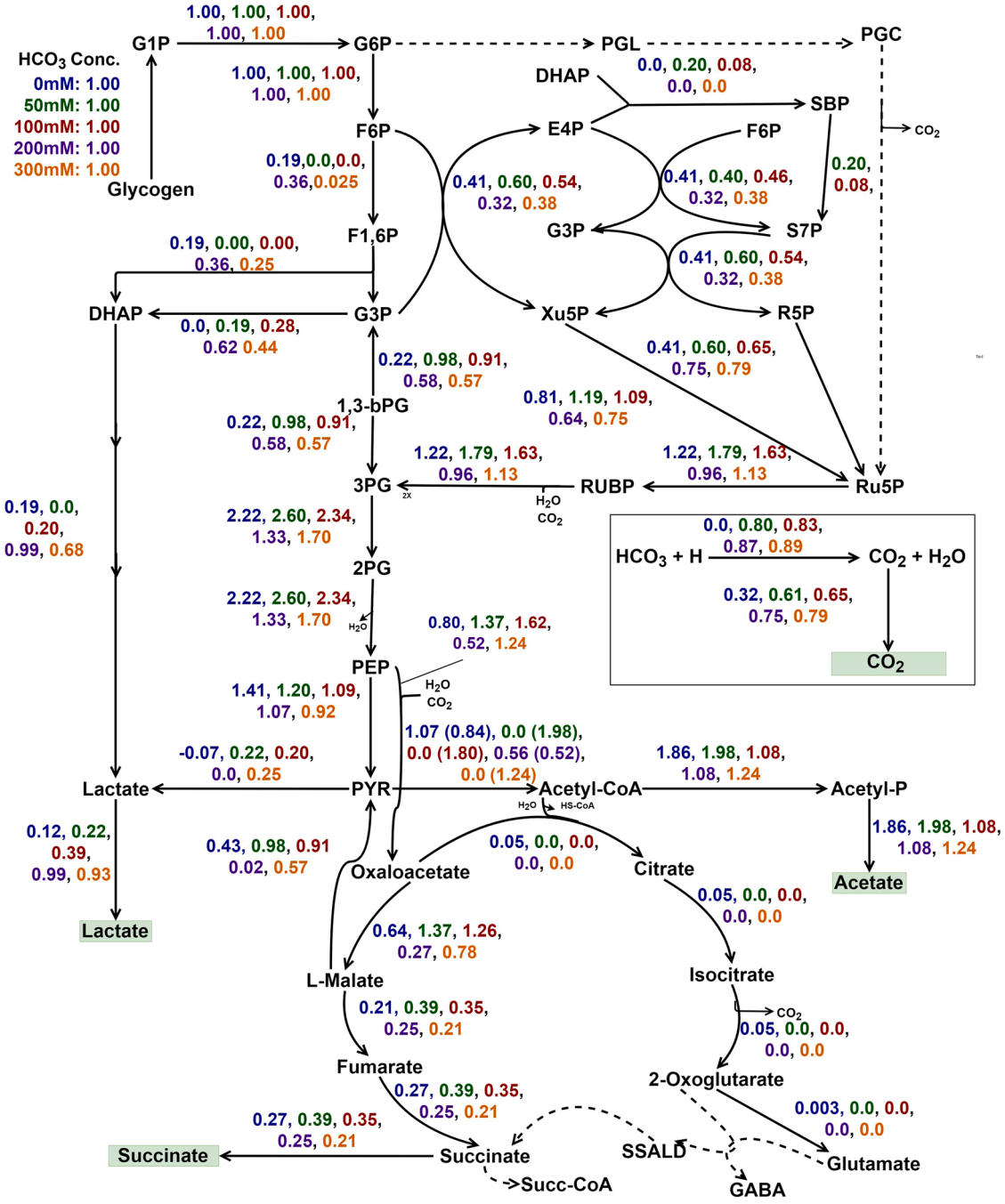

Fig. 7. Distribution of fluxes in the central carbon metabolic pathway for the case of *SC* 6803 subject to dark anoxic conditions at 30 °C and supplemented with different concentrations of $NaHCO_3$. Note that the fluxes were normalized with the corresponding absolute glycogen breakdown flux. The absolute glycogen breakdown flux for 0, 50, 100, 200 and 300 mM $NaHCO_3$ supplementation, respectively are 0.015, 0.013, 0.018, 0.029, and 0.031 mmol/gDW/h. Flux reported for the biochemical reaction PYR to acetyl-CoA includes contributions due to enzymes PDH and POR_Syn.

increases carbon flow from PEP to OAA and further to succinate through the TCA cycle reductive pathway. This could be because Malate dehydrogenase is active in TCA cycle secreting malate along with succinate which facilitates reductive pathway rather than the oxidative one. Malate dehydrogenase in *SC* 6803 is likely to have low activity in oxidative pathway [42]. The above strategy led to 1.2 fold increase in the succinate yield as compared to that observed in wild-type cells grown in NH_4Cl rich media (Table 1). Under the conditions of *ppc* overexpression, in addition to enhanced flux through the reductive pathway, the extent of gluconeogenesis remains at the same level as that for the wild-type.

We next asked the question what is the maximum theoretical succinate yield and the ensuing metabolic engineering strategies to achieve the same. Our analysis showed that the maximum theoretical succinate yield is 0.47, which is 1.8 fold higher than that achieved in the case of wild-type. Even for this maximum theoretical yield, the flux through gluconeogenesis decreased with further increase in the flux through PPC metabolic reaction. Interestingly, the TCA cycle is oxidative and the succinate synthesis is through the GABA shunt unlike the case observed in experiments in Hasunuma et al. [21,22]. The reduction in gluconeogenesis requires independent control of the redox balance which occurs through the oxidative pathway of TCA cycle and is catalyzed by trans-hydrogenase. The carbon that is now recovered due to lowered gluconeogenesis is channeled into the TCA cycle and thereby leading to an increase in succinate yield. This immediately suggests that an

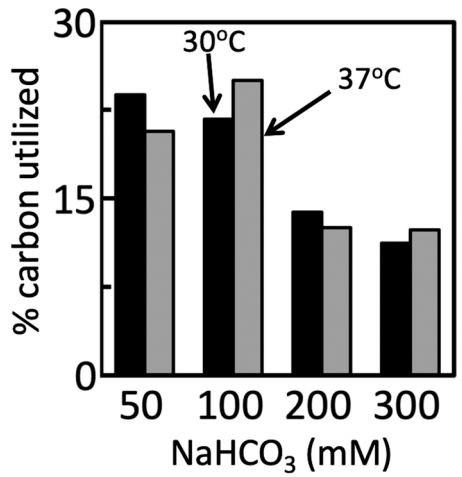

Fig. 8. Utilization of carbon from supplemented $NaHCO_3$ at different concentrations and at temperatures 30 °C and 37 °C.

appropriate metabolic engineering strategy to improve succinate yield is to simultaneously overexpress *ppc* and trans-hydrogenase enzymes, and block the reductive pathway of the TCA cycle, that is, deletion of malate dehydrogenase to arrest flux from OAA to malate. An important observation is that inspite of maximizing succinate the simultaneous accumulation of acetate as a by-product is inevitable due to its energy requirements. Iijima et al. [43] showed that by overexpression of Malate dehydrogenase (MDH) with 3 days of aerobic growth under light conditions followed by 3 days of dark anoxic fermentation of *SC* 6803 yielded 0.21 g/g of succinate per equivalent glucose, which is half of the theoretical maximum of 0.47 g/g of equivalent glucose obtained by our flux analysis. Hidese et al. [44] reported that *SC* 6803 over-expressing MDH subject to dark anoxic conditions led to 18 mg/gDW of succinate which is equivalent to 24% of the theoretical maximum predicted (Fig. 4).

With respect to the other organic acids, the maximum theoretical yield for acetate, lactate and malate are 3, 2, and 0.42, respectively. Accumulation of acetate and lactate inactivates the TCA cycle and minimizes gluconeogenesis. As a direct consequence, the species demonstrates the possibility of being homo-acetate or homo-lactate. Further, note that due to slow glycogen breakdown the productivity of acetate and lactate using dark anoxic conditions of cyanobacteria will be 0.13 and 0.09 mmol/gDW/h, respectively (assuming a glycogen breakdown of 0.0451 $mmol/gDW/h$ corresponding to *ppc* overexpression at 37 °C). In a recent study [44], lactate yield of 0.386 g/gDW was achieved in MDH over-expressed *SC* 6803, which is 50% of the theoretical maximum predicted by our model (Fig. S7). A direct comparison of these quantities with the existing processes for producing acetate and lactate using homo-acetate and homo-lactate organisms clearly indicates that scope for use of cyanobacteria to produce these is highly limited. However, use of this species for production of malate could be promising. Our analysis shows that in order to produce malate, flux of carbon from glycogen must be primarily channeled through the glycolysis and via the parallel route of DHAP to PYR. This ensures simultaneous stoichiometric accumulation of both PYR and PEP in order to channel the carbon towards malate. The potential metabolic engineering strategy could be to overexpress the enzymes facilitating flux in the DHAP to PYR pathway, in addition to over-expression of *ppc* gene. Note that inspite of employing these interventional approaches, the species will not serve as homo-malate as the production of acetate, though in relatively lesser quantities, cannot be avoided.

The analysis presented above points to the reductive pathway of the TCA cycle playing a dominant role in accumulation of organic acids. PEP to OAA biochemical reaction catalyzed by PEP carboxylase also requires CO_2 as an additional substrate. An overexpression of PEP carboxylase although increases flux through this reaction, the theoretical maximum cannot be achieved due to limitation of CO_2. In order to circumvent this limitation, addition of $NaHCO_3$ as a supplement under dark anoxic conditions could further enhance the flux through the PEP carboxylase and thereby maximizing the accumulation of organic acids. Nodal analysis suggests that the flux from glycogen through glycolysis reaches reductive pathway of the TCA cycle via OAA. Further, a part of it is recycled to acetate via malate and PYR through the malic enzyme (Fig. 9). This carbon ends up as acetate satisfying the energy requirements. On the other hand, accumulation of lactate is primarily due to routing of carbon via DHAP. It is noted that while the accumulation of glycogen occurs during the growth phase, increasing temperature led to an increase in the glycogen breakdown rate and thereby increasing the

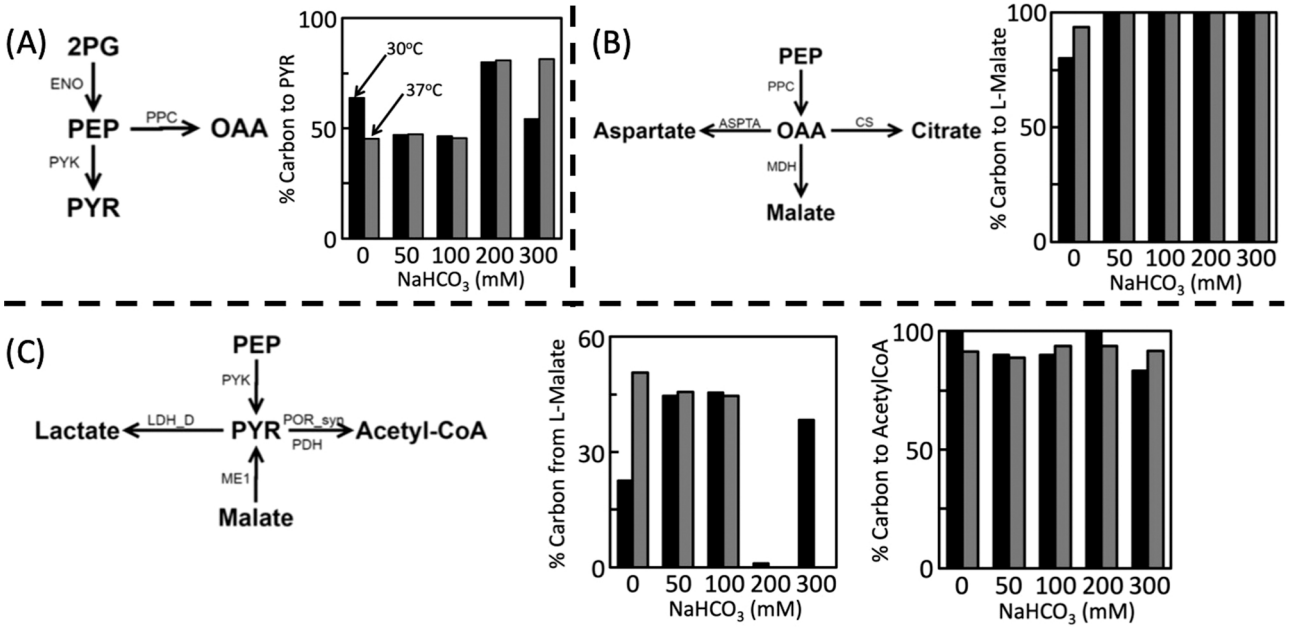

Fig. 9. Distribution of flux at (A) PEP, (B) OAA, and (C) PYR nodes in the central metabolic pathway causing channeling carbon to different organic acids when supplemented with sodium bicarbonate at 30 °C and 37 °C under dark anoxic conditions. Normalized fluxes used are those reported in Figs. 7 and S9.

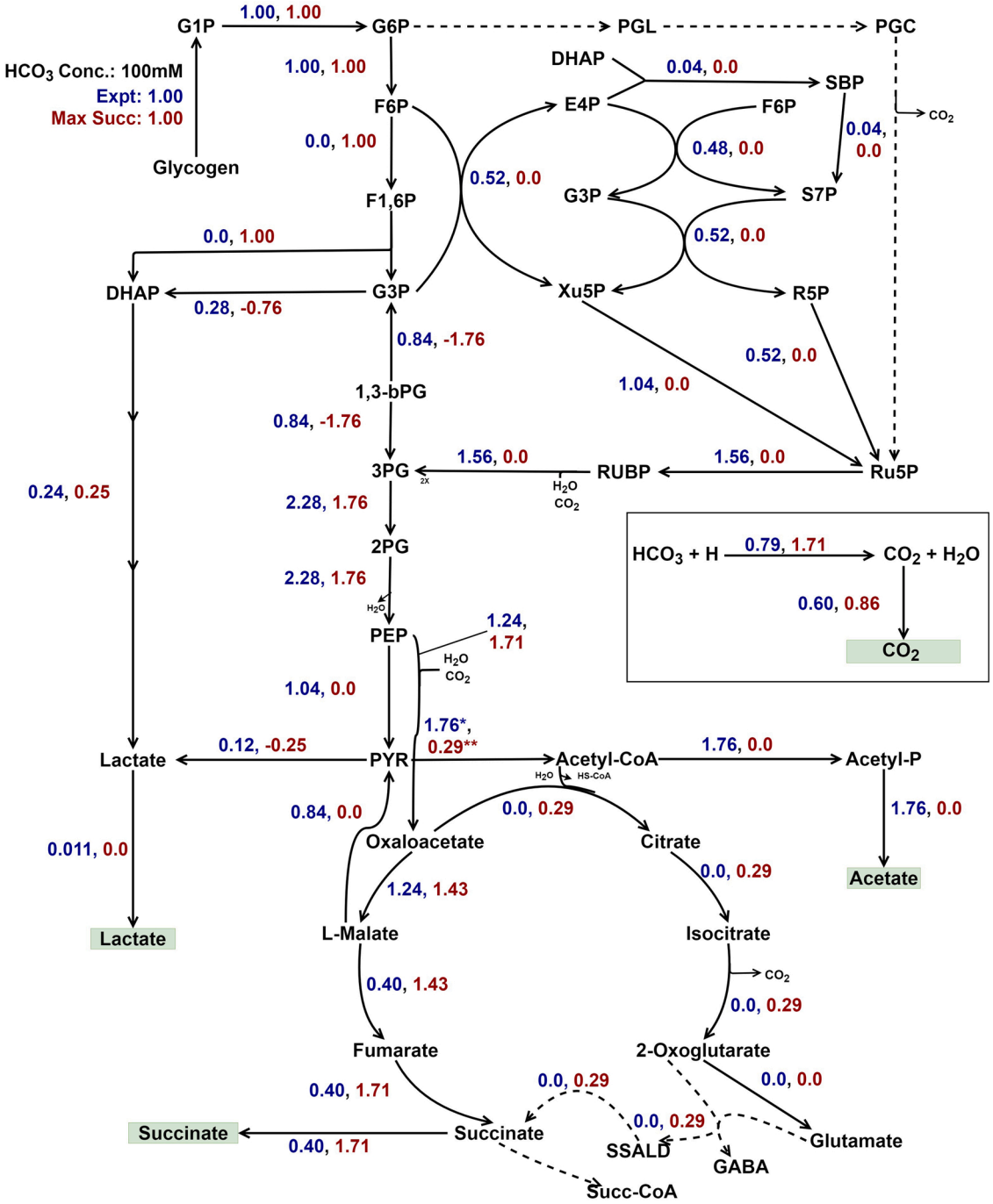

Fig. 10. Flux distribution map corresponding to the theoretical maximum succinate production for 100 mM $NaHCO_3$ supplementation at 37 °C. Fluxes were normalized with the corresponding absolute glycogen breakdown flux of 0.030 mmol/gDW/h. Note that the flux reported for PYR to acetyl-CoA includes those catalyzed by both PDH and POR_Syn.

absolute flux towards different organic acids under dark anoxic conditions. It is observed that only about 15–20% of the carbon from $NaHCO_3$ is utilized to supplement the biochemical reactions and remaining released as CO_2 (Fig. 8). However, the overall relative flux distribution with respect to glycogen uptake achieved for sodium bicarbonate supplement at 37 °C is similar to that obtained for the case of 30 °C (Figs. 7 and S9). It is seen that at higher $NaHCO_3$ concentrations, there is a significant reduction in the recycle of carbon to PYR from malate through malic enzyme resulting in decrease of the acetate yield. In summary, addition of 100 *mM* $NaHCO_3$ at 37 °C offers ~ 2.2 fold increase in the succinate production with substantial accumulation of both acetate and lactate (Fig. 6). At high concentrations of $NaHCO_3$, CO_2 utilization reaches a saturation and therefore most of the carbon from glycogen results in lactate production. A combined strategy of supplementation with $NaHCO_3$ and increased temperature can at best offer ~ 25% of the theoretical maximum succinate production (Fig. 10). Our analysis shows that this can be achieved only when fluxes to acetate and lactate are zero and the ATP requirement is satisfied through the oxidative pathway of the TCA cycle (Fig. 10).

5. Conclusions

In this study, we present a validated predictive genome-scale metabolic model for synthesis of organic acids by *Synechocystis* sp. PCC 6803

using dark anoxic fermentation of the glycogen accumulated during growth under photoautotrophic atmospheric CO_2 sequestering conditions. Using the model, we theoretically show that the yield for organic acids can be improved further by employing metabolic engineering strategies. In particular, we identify specific pathway engineering to increase the yield of succinate and malate. Overexpressing transhydrogenase along with *ppc* and also blocking the reductive pathway could improve succinate production. While overexpressing enzymes in the DHAP to PYR pathway maybe needed for improving malate yield, *SC* 6803 has the potential to be engineered into a home-lactate or homoacetate. Our analysis shows that sodium bicarbonate supplementation leads to enhancement in succinate production by not only providing additional carbon source but also removing the bottleneck for CO_2 requirement. Although challenging, a successful demonstration of these metabolic interventions needs to be complemented with strategies for improving glycogen breakdown rate which controls the overall productivity. A promising strategy to improve the glycogen breakdown rate is to increase the temperature.

CRediT authorship contribution statement

KJ: Data curation, Formal analysis, Methodology, Validation, Visualization, Writing – original draft. **SS:** Methodology, Formal analysis, Writing – original draft, Funding acquisition. **GV and KVV:** Conceptualization, Formal analysis, Funding acquisition, Investigation, Project administration, Resources, Supervision, Writing – original draft, Writing – review & editing.

Declaration of Competing Interest

The authors declare that they have no known competing financial interests or personal relationships that could have appeared to influence the work reported in this paper.

Acknowledgements

This work was funded by a grant Department of Biotechnology (DBT), Ministry of Science and Technology, Government of India [Grant no.: BT/EB/PAN IIT/2012] and by the Department of Science and Technology (DST) Women Scientists-A (WOS-A) Fellowship grant, Government of India [Grant no: SR/WOS-A/ET-58/2017].

Appendix A. Supporting information

Supplementary data associated with this article can be found in the online version at doi:10.1016/j.bej.2021.108297.

References

[1] C.J. Knoot, J. Ungerer, P.P. Wangikar, H.B. Pakrasi, Cyanobacteria: promising biocatalysts for sustainable chemical production, J. Biol. Chem. 293 (14) (2018) 5044–5052.
[2] M.C. Lai, E.I. Lan, Advances in metabolic engineering of cyanobacteria for photosynthetic biochemical production, Metabolites 5 (4) (2015) 636–658.
[3] Y. Hirokawa, Y. Maki, T. Hanai, Improvement of 1, 3-propanediol production using an engineered cyanobacterium, Synechococcus elongatus by optimization of the gene expression level of a synthetic metabolic pathway and production conditions, Metab. Eng. 39 (2017) 192–199.
[4] X. Liu, J. Sheng, R. Curtiss III, Fatty acid production in genetically modified cyanobacteria, Proc. Natl. Acad. Sci. USA 108 (17) (2011) 6899–6904.
[5] P. Lindberg, S. Park, A. Melis, Engineering a platform for photosynthetic isoprene production in cyanobacteria, using synechocystis as the model organism, Metab. Eng. 12 (1) (2010) 70–79.
[6] J.W. Oliver, I.M. Machado, H. Yoneda, S. Atsumi, Cyanobacterial conversion of carbon dioxide to 2, 3-butanediol, Proc. Natl. Acad. Sci. USA 110 (4) (2013) 1249–1254.
[7] E.I. Lan, J.C. Liao, Metabolic engineering of cyanobacteria for 1-butanol production from carbon dioxide, Metab. Eng. 13 (4) (2011) 353–363.
[8] L. Wang, L. Chen, S. Yang, X. Tan, Photosynthetic conversion of carbon dioxide to oleochemicals by cyanobacteria: recent advances and future perspectives, Front. Microbiol. 11 (2020).
[9] Y.-N. Choi, J.W. Lee, J.W. Kim, J.M. Park, Acetyl-coa-derived biofuel and biochemical production in cyanobacteria: a mini review, J. Appl. Phycol. 32 (2020) 1643–1656.
[10] I. Martinez, H. Gao, G.N. Bennett, K.-Y. San, High yield production of four-carbon dicarboxylic acids by metabolically engineered Escherichia coli, J. Ind. Microbiol. Biotechnol. 45 (1) (2018) 53–60.
[11] J.-w. Kim, J.H. Jang, H.J. Yeo, J. Seol, S.R. Kim, Y.H. Jung, Lactic acid production from a whole slurry of acid-pretreated spent coffee grounds by engineered Saccharomyces cerevisiae, Appl. Biochem. Biotechnol. 189 (1) (2019) 206–216.
[12] Z. Liu, K. Wang, Y. Chen, T. Tan, J. Nielsen, Third-generation biorefineries as the means to produce fuels and chemicals from Co_2, Nat. Catal. 3 (3) (2020) 274–288.
[13] T. Osanai, T. Shirai, H. Iijima, Y. Nakaya, M. Okamoto, A. Kondo, M.Y. Hirai, Genetic manipulation of a metabolic enzyme and a transcriptional regulator increasing succinate excretion from unicellular cyanobacterium, Front. Microbiol. 6 (2015) 1064.
[14] S.G. Ball, M.K. Morell, From bacterial glycogen to starch: understanding the biogenesis of the plant starch granule, Annu. Rev. Plant Biol. 54 (1) (2003) 207–233.
[15] M. Cano, S.C. Holland, J. Artier, R.L. Burnap, M. Ghirardi, J.A. Morgan, J. Yu, Glycogen synthesis and metabolite overflow contribute to energy balancing in cyanobacteria, Cell Rep. 23 (3) (2018) 667–672.
[16] M. Gründel, R. Scheunemann, W. Lockau, Y. Zilliges, Impaired glycogen synthesis causes metabolic overflow reactions and affects stress responses in the cyanobacterium synechocystis sp. pcc 6803, Microbiology 158 (12) (2012) 3032–3043.
[17] T. Hasunuma, F. Kikuyama, M. Matsuda, S. Aikawa, Y. Izumi, A. Kondo, Dynamic metabolic profiling of cyanobacterial glycogen biosynthesis under conditions of nitrate depletion, J. Exp. Bot. 64 (10) (2013) 2943–2954.
[18] M. Lehmann, G. Wöber, Accumulation, mobilization and turn-over of glycogen in the blue-green bacterium Anacystis nidulans, Arch. Microbiol. 111 (1–2) (1976) 93–97.
[19] S. Shinde, X. Zhang, S.P. Singapuri, I. Kalra, X. Liu, R.M. Morgan-Kiss, X. Wang, Glycogen metabolism supports photosynthesis start through the oxidative pentose phosphate pathway in cyanobacteria, Plant Physiol. 182 (1) (2020) 507–517.
[20] S. Ueda, Y. Kawamura, H. Iijima, M. Nakajima, T. Shirai, M. Okamoto, A. Kondo, M.Y. Hirai, T. Osanai, Anionic metabolite biosynthesis enhanced by potassium under dark, anaerobic conditions in cyanobacteria, Sci. Rep. 6 (1) (2016) 1–9.
[21] T. Hasunuma, M. Matsuda, A. Kondo, Improved sugar-free succinate production by synechocystis sp. pcc 6803 following identification of the limiting steps in glycogen catabolism, Metab. Eng. Commun. 3 (2016) 130–141.
[22] T. Hasunuma, M. Matsuda, Y. Kato, C.J. Vavricka, A. Kondo, Temperature enhanced succinate production concurrent with increased central metabolism turnover in the cyanobacterium synechocystis sp. pcc 6803, Metab. Eng. 48 (2018) 109–120.
[23] C. Durall, K. Kukil, J.A. Hawkes, A. Albergati, P. Lindblad, P. Lindberg, Production of succinate by engineered strains of synechocystis pcc 6803 overexpressing phosphoenolpyruvate carboxylase and a glyoxylate shunt, Microb. Cell Factor. 20 (1) (2021) 1–14.
[24] L.T. Guerra, Y. Xu, N. Bennette, K. McNeely, D.A. Bryant, G.C. Dismukes, Natural osmolytes are much less effective substrates than glycogen for catabolic energy production in the marine cyanobacterium synechococcus sp. strain pcc 7002, J. Biotechnol. 166 (3) (2013) 65–75.
[25] A.A. Shastri, J.A. Morgan, Flux balance analysis of photoautotrophic metabolism, Biotechnol. Prog. 21 (6) (2005) 1617–1626.
[26] S.-J. Hong, C.-G. Lee, Evaluation of central metabolism based on a genomic database ofsynechocystis pcc6803, Biotechnol. Bioprocess Eng. 12 (2) (2007) 165–173.
[27] J. Nogales, S. Gudmundsson, E.M. Knight, B.O. Palsson, I. Thiele, Detailing the optimality of photosynthesis in cyanobacteria through systems biology analysis, Proc. Natl. Acad. Sci. USA 109 (7) (2012) 2678–2683.
[28] P. Fu, Genome-scale modeling of synechocystis sp. pcc 6803 and prediction of pathway insertion, J. Chem. Technol. Biotechnol.: Int. Res. Process Environ. Clean Technol. 84 (4) (2009) 473–483.
[29] A. Montagud, E. Navarro, P.F. de Córdoba, J.F. Urchueguía, K.R. Patil, Reconstruction and analysis of genome-scale metabolic model of a photosynthetic bacterium, BMC Syst. Biol. 4 (1) (2010) 156.
[30] A. Montagud, A. Zelezniak, E. Navarro, P.F. de Córdoba, J.F. Urchueguía, K. R. Patil, Flux coupling and transcriptional regulation within the metabolic network of the photosynthetic bacterium synechocystis sp. pcc6803, Biotechnol. J. 6 (3) (2011) 330–342.
[31] H. Knoop, Y. Zilliges, W. Lockau, R. Steuer, The metabolic network of synechocystis sp. pcc 6803: systemic properties of autotrophic growth, Plant Physiol. 154 (1) (2010) 410–422.
[32] K. Yoshikawa, Y. Kojima, T. Nakajima, C. Furusawa, T. Hirasawa, H. Shimizu, Reconstruction and verification of a genome-scale metabolic model for synechocystis sp. pcc6803, Appl. Microbiol. Biotechnol. 92 (2) (2011) 347.
[33] R. Saha, A.T. Verseput, B.M. Berla, T.J. Mueller, H.B. Pakrasi, C.D. Maranas, Reconstruction and comparison of the metabolic potential of cyanobacteria cyanothece sp. atcc 51142 and synechocystis sp. pcc 6803, PLoS One 7 (10) (2012), e48285.
[34] C.J. Joshi, C.A. Peebles, A. Prasad, Modeling and analysis of flux distribution and bioproduct formation in synechocystis sp. pcc 6803 using a new genome-scale metabolic reconstruction, Algal Res. 27 (2017) 295–310.
[35] R. Hidese, M. Matsuda, T. Osanai, T. Hasunuma, A. Kondo, Malic enzyme facilitates D-lactate production through increased pyruvate supply during anoxic dark fermentation in synechocystis sp. pcc 6803, ACS Synth. Biol. 9 (2) (2020) 260–268.

[36] A. Rohatgi, Webplotdigitizer: Version 4.2, 2019. ⟨https://automeris.io/WebPlotDigitizer⟩.
[37] A. Ebrahim, J.A. Lerman, B.O. Palsson, D.R. Hyduke, Cobrapy: constraints-based reconstruction and analysis for python, BMC Syst. Biol. 7 (1) (2013) 74.
[38] J.D. Orth, I. Thiele, B. Palsson, What is flux balance analysis? Nat. Biotechnol. 28 (3) (2010) 245–248.
[39] R. Mahadevan, C.H. Schilling, The effects of alternate optimal solutions in constraint-based genome-scale metabolic models, Metab. Eng. 5 (4) (2003) 264–276.
[40] S. Gudmundsson, I. Thiele, Computationally efficient flux variability analysis, BMC Bioinform. 11 (1) (2010) 489.
[41] J.F. Andrews, A mathematical model for the continuous culture of microorganisms utilizing inhibitory substrates, Biotechnol. Bioeng. 10 (6) (1968) 707–723.
[42] M. Takeya, S. Ito, H. Sukigara, T. Osanai, Purification and characterisation of malate dehydrogenase from synechocystis sp. pcc 6803: biochemical barrier of the oxidative tricarboxylic acid cycle, Front. Plant Sci. 9 (2018) 947.
[43] H. Iijima, A. Watanabe, H. Sukigara, K. Iwazumi, T. Shirai, A. Kondo, T. Osanai, Four-carbon dicarboxylic acid production through the reductive branch of the open cyanobacterial tricarboxylic acid cycle in synechocystis sp. pcc 6803, Metab. Eng. 65 (2021) 88–98.
[44] R. Hidese, M. Matsuda, T. Osanai, T. Hasunuma, A. Kondo, Malic enzyme facilitates D-lactate production through increased pyruvate supply during anoxic dark fermentation in synechocystis sp. pcc 6803, ACS Synth. Biol. 9 (2020) 260–268.